Fulde-Ferrell-Larkin-Ovchinnikov state in a superconducting thin film attached to a ferromagnetic cluster

Shu-Ichiro Suzuki [1], Takumi Sato,[2] Alexander A. Golubov,[1] and Yasuhiro Asano [2]

[1]*Faculty of Science and Technology and MESA+ Institute for Nanotechnology, University of Twente, 7500 AE Enschede, The Netherlands*
[2]*Department of Applied Physics, Hokkaido University, Sapporo 060-8628, Japan*

We study theoretically the Fulde-Ferrell-Larkin-Ovchinnikov (FFLO) states appearing locally in a superconducting thin film with a small circular magnetic cluster. By solving the Eilenberger equation in two dimensions, we calculate the pair potential, pairing correlations, free-energy density, and quasiparticle density of states for various cluster sizes and exchange potentials. Increasing the exchange potential and cluster size leads to a higher number of nodes in the pair potential. Although the free-energy density beneath the ferromagnet locally exceeds the normal-state value, the FFLO states are stabilized by the superconducting condensate away from the magnetic cluster. Analyzing the pairing-correlation functions, we show that the spatial variation of the spin-singlet *s*-wave pair potential generates *p*-wave Cooper pairs. These odd-frequency Cooper pairs play a dominant role in governing the inhomogeneous subgap spectra observed in the local density of states. Furthermore, we propose an experimental method for the detection of local FFLO states by analyzing the quasiparticle density of states.

I. INTRODUCTION

In the presence of a Zeeman field, a spin-singlet Cooper pair has center-of-mass momentum, causing the oscillation in the superconducting pair potential in real space. These oscillating superconducting states, known as Fulde-Ferrell [1] (FF) and Larkin-Ovchinnikov [2] (LO) states, were proposed in the 1960s but remained elusive until recently. Several experiments have indicated the possibility of observing the FFLO state in layered organic superconductors [3–10], FeSe [11,12], and other materials [13,14]. Theoretical studies [15,16] have suggested that the oscillation of the pair potential makes the superconducting state unstable. On the other hand, the oscillation of *pairing correlations* has been extensively discussed in superconductor/ferromagnet (SF) junctions [17–21]. Although the pair potential is absent in a ferromagnet, the proximity effect allows nonzero pairing correlations. The success of these studies highlights SF junctions as a suitable system for investigating the nature of FFLO states. For instance, in recent experiments [22–24], a superconducting state with a significant exchange potential was achieved by creating a hybrid structure consisting of a circular ferromagnetic cluster attached to a thin superconducting film. This configuration suggests the possibility of the formation of a localized FFLO state within the superconducting region beneath the ferromagnetic cluster.

The effects of magnetic objects embedded in a superconductor on superconducting states have been studied since the 1960s. It is well established that magnetic impurities decrease the superconducting transition temperature T_c [25], form an impurity band below the superconducting gap [26–29], and are an element for realizing the topologically nontrivial superconducting state [30,31]. These effects depend not only on the impurity concentration and the amplitude of the magnetic moments. The size of a magnetic object is also an important factor. A pointlike magnetic impurity suppresses the pair potentials locally but the suppression in not significant [32,33]. An finite-size magnetic cluster, on the other hand, changes the sign of the pair potential [34–37]. In our previous paper [37], we have shown that odd-frequency Cooper pairs surrounding the magnetic cluster are responsible for the sign change of the pair potential [38,39]. It is widely accepted that odd-frequency Cooper pairs exist locally in various SF hybrid structures [40] and play an essential role in various physical phenomena. For instance, the Josephson current through a half-metallic ferromagnet [41–48] is attributed to odd-frequency pairs induced in the ferromagnet. However, the effects of odd-frequency Cooper pairs on the FFLO state are currently not well understood. We address this issue in the present paper.

We study the characteristic features of the local FFLO states in a superconducting thin film to which a circular magnetic cluster is attached (see Fig. 1). Using the Eilenberger theory, we calculate the pair potential, the pairing correlation functions, the free-energy density, and the quasiparticle local density of states (LDOS) for several choices of the cluster
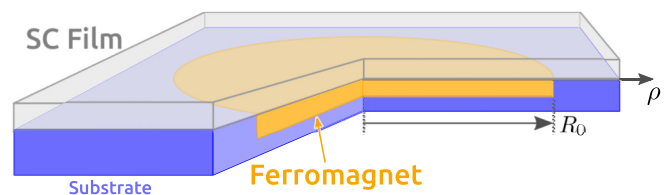

FIG. 1. Schematic illustration of the system. A thin film of an *s*-wave superconductor is deposited on a circular-shaped magnetic cluster. The radius of the magnetic cluster R_0 is of the order of the coherence length ξ_0.

size and exchange potential. The results indicate that the superconducting condensate away from the magnetic segment stabilizes the local FFLO states. We also conclude that odd-frequency Cooper pairs support the sign change of the pair potential in real space and govern the inhomogeneous subgap spectra of the LDOS.

This paper is organized as follows. In Sec. II, we explain an SF structure considered in this paper and theoretical tools to analyze the superconducting state. We discuss the numerical results in two dimensions in Sec. III. We also discuss numerical results in one dimension in Sec. IV. The conclusions are given in Sec. V.

II. MODEL AND FORMULATION

We consider the hybrid structure shown in Fig. 1. A circular magnetic cluster is attached to an infinitely large superconducting thin film in the x-y plane. The effects of the magnetic cluster are considered through the exchange potential proximities into the superconducting film,

$$V(\boldsymbol{r}) = V_0 \Theta(R_0 - \rho) \boldsymbol{e}_z, \tag{1}$$

where $\rho = \sqrt{x^2 + y^2}$ and R_0 is the radius of the magnetic cluster and $\Theta(\rho)$ is the Heaviside step function. Therefore, $\rho = R_0$ indicates the boundary between the magnetic segment and the nonmagnetic segment on the superconducting thin film.

We examine the properties of the superconducting states utilizing the quasiclassical Eilenberger theory [49]. The Green's functions obey the Eilenberger equation:

$$i\boldsymbol{v}_F \cdot \boldsymbol{\nabla} \check{g} + [i\omega_n \check{\tau}_3 + \check{H}, \check{g}]_- = 0, \tag{2}$$

$$\check{g} = \begin{pmatrix} \hat{g} & \hat{f} \\ -\hat{\underline{f}} & -\hat{\underline{g}} \end{pmatrix}, \quad \check{H} = \begin{pmatrix} \boldsymbol{V} \cdot \hat{\boldsymbol{\sigma}} & \hat{\Delta} \\ \hat{\underline{\Delta}} & \boldsymbol{V} \cdot \hat{\boldsymbol{\sigma}}^* \end{pmatrix}, \tag{3}$$

where $\check{g} = \check{g}(\boldsymbol{r}, \boldsymbol{k}, i\omega_n)$ is the quasiclassical Green's function in the Matsubara representation, $\hat{\Delta}(\boldsymbol{r})$ is the pair potential, $\boldsymbol{v}_F = v_F \boldsymbol{k}$ is the Fermi velocity, and we assume the junction is in equilibrium. The *undertilde* function

$$\underline{\hat{K}}(\boldsymbol{r}, \boldsymbol{k}, i\omega_n) \equiv \hat{K}^*(\boldsymbol{r}, -\boldsymbol{k}, i\omega_n) \tag{4}$$

represents particle-hole conjugation of $\hat{K}(\boldsymbol{r}, \boldsymbol{k}, i\omega_n)$, where the unit vector $\boldsymbol{k}$ points the direction of the Fermi momentum. In this paper, the accents $\check{}$ and $\hat{}$ mean matrices in particle hole and those in spin space, respectively. The Pauli matrices in these spaces are denoted by $\check{\tau}_j$ and $\hat{\sigma}_j$ with $j \in \{1, 2, 3\}$. The identity matrices are represented by $\check{\tau}_0$ and $\hat{\sigma}_0$. Throughout this paper, we use the system of units $\hbar = k_B = c = 1$, where k_B is the Boltzmann constant and c is the speed of light.

The Eilenberger equation (2) can be simplified by the Riccati parametrization [50–53]. The Green's function can be expressed in terms of the coherence function $\hat{\gamma} = \hat{\gamma}(\boldsymbol{r}, \boldsymbol{k}, i\omega_n)$:

$$\check{g} = 2 \begin{pmatrix} \hat{\mathcal{G}} & \hat{\mathcal{F}} \\ -\hat{\underline{\mathcal{F}}} & -\hat{\underline{\mathcal{G}}} \end{pmatrix} - \check{\tau}_3, \tag{5}$$

$$\hat{\mathcal{G}} = (1 - \hat{\gamma}\hat{\underline{\gamma}})^{-1}, \quad \hat{\mathcal{F}} = (1 - \hat{\gamma}\hat{\underline{\gamma}})^{-1}\hat{\gamma}. \tag{6}$$

The equation for $\hat{\gamma}$ is reduced into the Riccati-type differential equation:

$$(i\boldsymbol{v}_F \cdot \boldsymbol{\nabla} + 2i\omega_n)\hat{\gamma} + (\boldsymbol{V} \cdot \hat{\boldsymbol{\sigma}})\hat{\gamma} - \hat{\gamma}(\boldsymbol{V} \cdot \hat{\boldsymbol{\sigma}}^*) - \hat{\Delta} + \hat{\gamma}\hat{\underline{\Delta}}\hat{\gamma} = 0. \tag{7}$$

For a spin-singlet s-wave superconductor ($\hat{\Delta} = \Delta i\hat{\sigma}_2$) under the exchange potential in Eq. (1), the anomalous Green's function and the coherence function are represented by

$$\hat{f} = i(f_0 + f_3\hat{\sigma}_3)\hat{\sigma}_2, \quad \hat{\underline{f}} = -i\hat{\sigma}_2(\underline{f}_0 + \underline{f}_3\hat{\sigma}_3), \tag{8}$$

$$\hat{\gamma} = i(\gamma_0 + \gamma_3\hat{\sigma}_3)\hat{\sigma}_2, \quad \hat{\underline{\gamma}} = -i\hat{\sigma}_2(\underline{\gamma}_0 + \underline{\gamma}_3\hat{\sigma}_3), \tag{9}$$

where $\underline{f}_0(\boldsymbol{k}) = -f_0^*(-\boldsymbol{k})$ and $\underline{f}_3(\boldsymbol{k}) = f_3^*(-\boldsymbol{k})$. Equation (7) can be reduced to

$$\boldsymbol{v}_F \cdot \boldsymbol{\nabla}\gamma_0 + 2(\omega_n\gamma_0 - iV\gamma_3) - \Delta + \Delta^*[\gamma_0^2 + \gamma_3^2] = 0, \tag{10}$$

$$\boldsymbol{v}_F \cdot \boldsymbol{\nabla}\gamma_3 + 2(\omega_n\gamma_3 - V\gamma_0) + \Delta^*[2\gamma_0\gamma_3] = 0, \tag{11}$$

The coherence functions far from the magnetic cluster (i.e., $\rho \gg R_0$), $\bar{\gamma}(\boldsymbol{k}, i\omega_n)$ is calculated as

$$\bar{\gamma}_0 = \frac{\bar{\Delta}}{\omega_n + \sqrt{\omega_n^2 + |\bar{\Delta}|^2}}, \quad \bar{\gamma}_3 = 0, \tag{12}$$

where $\bar{}$ means the value in the homogeneous region. In this paper, we assume the homogeneous superconductivity at $\rho \gg R_0$ [54].

The spatial profile of the pair potential is determined by the solving the gap equation self-consistently

$$\Delta(\boldsymbol{r}) = 2\lambda N_0 \frac{\pi}{i\beta} \sum_{\omega_n}^{\omega_c} \langle f_0(\boldsymbol{r}, \boldsymbol{k}', i\omega_n)\rangle, \tag{13}$$

$$\lambda = \frac{1}{2N_0} \left[\ln \frac{T}{T_c} + \sum_{n=0}^{n_c} \frac{1}{n + 1/2} \right]^{-1}, \tag{14}$$

where $\beta = 1/T$, T_c is the critical temperature, N_0 is the density of the states (DOS) in the normal state at the Fermi energy, ω_c is the high-energy cutoff, and $n_c = [\omega_c/2\pi T_c]$. The angle average on the Fermi surface is denoted by $\langle \cdots \rangle = \int_{-\pi}^{\pi} \cdots d\varphi_k/2\pi$, where $k_x = \cos\varphi_k$ and $k_y = \sin\varphi_k$ with φ_k being the azimuthal angle in the momentum space. The coordinate in real space is parametrized as $\boldsymbol{r} = (\rho\cos\phi_r, \rho\sin\phi_r)$. The LDOS can be calculated from the diagonal parts of the Green's function,

$$N(\boldsymbol{r}, \varepsilon) = N_0 \langle \text{Tr}[\hat{g}(\boldsymbol{r}, \boldsymbol{k}', i\omega_n)]\rangle|_{i\omega_n \to \varepsilon + i\delta}, \tag{15}$$

where δ is the smearing factor.

The pairing correlation function is decomposed into four dominant components. The spin-singlet s-wave component

$$f_0^{\text{SW}}(\rho, i\omega) = \frac{1}{2}\langle \text{Tr}[(i\hat{\sigma}_2)^\dagger \hat{f}(\rho, \boldsymbol{k}, i\omega_n)]\rangle \tag{16}$$

is the most dominant far from the magnetic cluster and is linked to the pair potential as shown in Eq. (13). The spin-triplet s-wave component

$$f_3^{\text{SW}}(\rho, i\omega) = \frac{1}{2}\langle \text{Tr}[(i\hat{\sigma}_3\hat{\sigma}_2)^\dagger \hat{f}(\rho, \boldsymbol{k}, i\omega_n)]\rangle \tag{17}$$

is generated by the exchange potential and belongs to an odd-frequency symmetry class. In what follows, we focus on
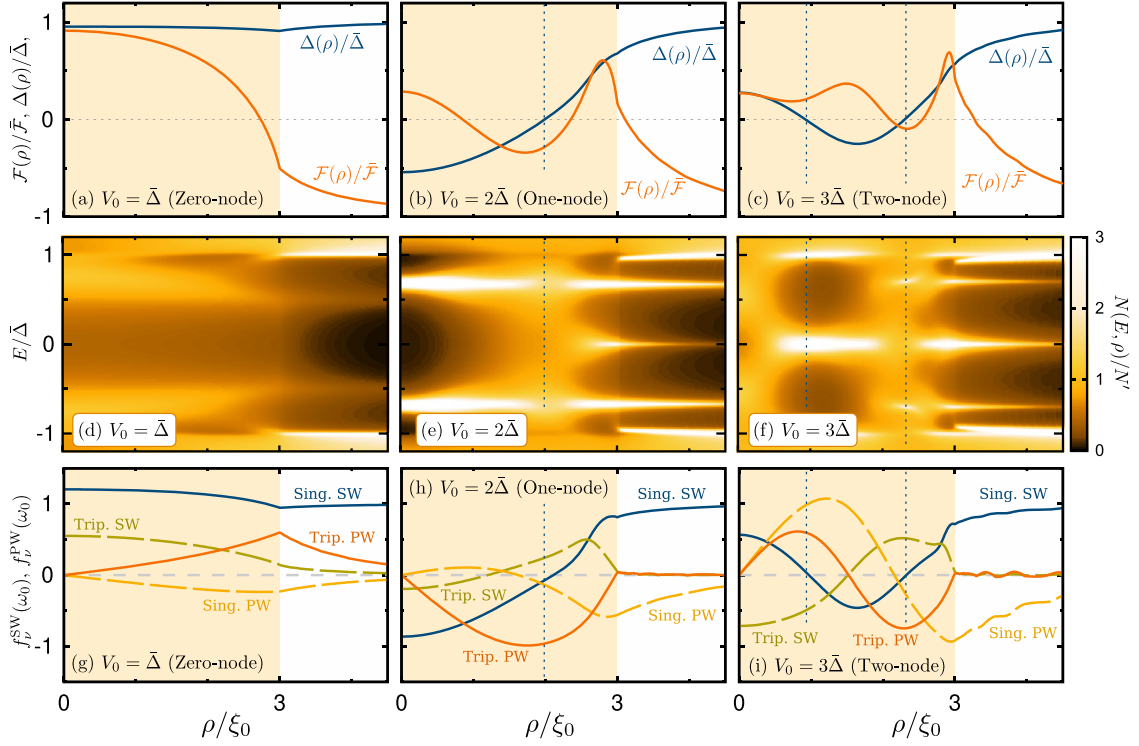
FIG. 2. Spatial profiles of the pair potential $\Delta(\rho)$ and free-energy density $\mathcal{F}(\rho)$ for (a) $V_0 = \bar{\Delta}$, (b) $2\bar{\Delta}$, and (c) $3\bar{\Delta}$. The results are normalized to their bulk values: $\bar{\Delta}$ and $\bar{\mathcal{F}}$. The positive free-energy density means that the normal state is stabler than a superconducting state locally. The vertical dotted lines indicate the places of nodes in the pair potential. The shaded areas indicate the area beneath the magnetic cluster with $R_0 = 3\xi_0$. Local densities of states (LDOS) for (d) $V_0 = \bar{\Delta}$, (e) $2\bar{\Delta}$, and (f) $3\bar{\Delta}$. The LDOS are normalized to $N' = 2N_0$. Pairing correlation functions for (g) $V_0 = \bar{\Delta}$, (h) $2\bar{\Delta}$, and (i) $3\bar{\Delta}$. The solid (broken) lines indicate the results of even-frequency (odd-frequency) pairing correlations. The temperature and the cutoff energy are set to $T = 0.2T_c$ and $\omega_c = 6\pi T_c$.

$\phi_r = 0$ because these components are isotropic in real space and independent of ϕ_r. In addition to s-wave components, odd-parity p-wave components also appear in the FFLO state since the spatial variation of the pair potential breaks inversion symmetry locally [55]. Along the x axis, two p_x-wave components are generated as a result of breaking inversion symmetry in the x direction: spin-singlet p_x-wave component f_0^{PW} and spin-triplet p_x-wave component f_3^{PW} defined by

$$f_\nu^{\mathrm{PW}}(\rho, i\omega) = \frac{1}{2}\langle 2k_x \mathrm{Tr}[(i\hat{\sigma}_\nu\hat{\sigma}_2)^\dagger \hat{f}(\rho, \boldsymbol{k}, i\omega_n)]\rangle. \quad (18)$$

The free-energy density $\mathcal{F}(\boldsymbol{r})$ can be calculated from the Green's function as [37,56,57]

$$\mathcal{F} = \mathcal{F}_f + \mathcal{F}_g, \quad (19)$$

$$\mathcal{F}_f = \pi N_0 T \sum_{\omega_n} \langle \Delta^*(\boldsymbol{r}) f(\boldsymbol{r}, \boldsymbol{k}, i\omega_n)\rangle, \quad (20)$$

$$\mathcal{F}_g = 4\pi N_0 T \sum_{\omega_n>0}^{\omega_c} \int_{\omega_n}^{\omega_c'} \langle \mathrm{Re}[g(\boldsymbol{r}, \boldsymbol{k}, i\omega_n) - 1]\rangle, \quad (21)$$

where the free-energy density is measured from its normal value, $\mathcal{F} = \mathcal{F}_S - \mathcal{F}_N$. In a homogeneous SC, the free-energy density approaches $\mathcal{F}(\rho) \to -\bar{\mathcal{F}}$ at low temperature with $\bar{\mathcal{F}} = N_0\bar{\Delta}^2/2$ being the condensation energy in the bulk.

In the numerical simulations, we fix the parameters $\omega_c = 6\pi T_c$, $T = 0.2T_c$, $\delta = 0.01\bar{\Delta}$, and $\omega_c' = 100\bar{\Delta}$, with $\xi_0 = \hbar v_F/2\pi T_c$ being the coherence length.

III. NUMERICAL RESULTS

A. Pair potential and free-energy density

We first discuss the influences of the exchange potential on the pair potential as shown in Figs. 2(a)–2(c), where the spatial variations of the pair potential are plotted for $V_0/\bar{\Delta} = 1$ in (a), 2 in (b), and 3 in (c). The size of the magnetic cluster is $R_0 = 3\xi_0$. The pair potential is almost homogeneous when the magnetization is comparable to (or smaller than) the superconducting gap (i.e., $V_0 < \bar{\Delta}$) as shown in Fig. 2(a). We refer to this state as the zero-node state. For $V_0 = 2\bar{\Delta}$ [Fig. 2(b)], the pair potential is suppressed and changes its sign once around $\rho = 2\xi_0$ (one-node state). For $V = 3\bar{\Delta}$ [Fig. 2(c)], the pair potential changes the sign twice (two-node state): negative approximately at $1.0 < \rho/\xi_0 < 2.1$ and positive at $\rho/\xi_0 < 1.0$. Namely, the FFLO-like superconducting states are realized locally (i.e., only beneath the magnetic cluster).

In the presence of the Zeeman field, the condition for the uniform superconducting state is given by $V_0 < \bar{\Delta}/\sqrt{2}$ [58,59]. The superconducting state for $V_0 = \bar{\Delta}$ in Fig. 2(a), however, goes beyond this limit. The pair potentials in Figs. 2(a)–2(c) are self-consistently obtained as stable solutions of the Eilenberger equation. Such local FFLO states can be supported by the wide superconducting region outside the cluster. To confirm the validity of this argument, we calculate the free-energy density $\mathcal{F}(\rho)$ in Figs. 2(a)–2(c). The vertical axis is normalized to the condensation energy in a uniform superconductor $\bar{\mathcal{F}} = \bar{\Delta}^2 N_0/2$ at zero temperature. The

free-energy density outside the magnetic segment is negative (smaller than the free-energy density in the normal state) and approaches $-\bar{\mathcal{F}}$ for $\rho \gg R_0$. Inside the magnetic segment, on the other hand, the free-energy density becomes positive locally. In particular, the free-energy density at $V_0 = \bar{\Delta}$ in Fig. 2(a) is always positive at $\rho < R_0$. However, the total free energy $\mathcal{F}_{\text{Tot}} = \int \mathcal{F} d\boldsymbol{r}$ is always negative because of the massive superconducting region outside the cluster. Figures 2(b) and 2(c) show that introducing the nodes in the pair potential reduces the free-energy density at $\rho < R_0$ drastically. Even so, the free energy at the magnetic segment $\mathcal{F}_{\text{in}} = \int_{r<R_0} \mathcal{F} d\boldsymbol{r}$ remains positive in the local FFLO states. At $V_0 = 2\bar{\Delta}$ in Fig. 2(b), $\mathcal{F}$ has a dip at $\rho \sim 1.9\xi_0$ that corresponds to the place of the node in the pair potential. A similar behavior appears also in the results for $V_0 = 3\bar{\Delta}$ [Fig. 2(c)]. The nodes in the pair potential and the dips in the free-energy density appear almost at the same place. This correspondence, however, contradicts intuition: the free-energy density seems have a peak (local maximum) around a node because the quasiparticle excitations below $\bar{\Delta}$ are allowed. The results in Figs. 2(b) and 2(c), however, show the opposite tendency. In Sec. III C, we will explore this further and discuss how p-wave Cooper pairs localize at the nodes of the s-wave pair potential, influencing the behavior of the free-energy density.

B. Local density of states

The signatures of the local FFLO state are accessible through the LDOS of a quasiparticle which can be measured by the scanning tunnel spectroscopy (STS) technique. The numerical results of the LDOS are shown in Figs. 2(d)–2(f), where the exchange potentials are $V_0/\bar{\Delta} = 1$ in (d), 2 in (e), and 3 in (f). The contour plots are shown as a function of the energy of a quasiparticle E and the radius ρ.

At $V_0 = \bar{\Delta}$, the pair potential is almost homogeneous as shown in Fig. 2(a). The LDOS beneath the magnetic cluster indicates the appearance of quasiparticle states below the gap. The exchange potential pushes the coherence peaks down to the subgap region ($|E| < \bar{\Delta}$) and broadens them in energy. As a result, the LDOS is slightly enhanced around $E = 0.7\bar{\Delta}$. These states are related to the Yu-Shiba-Rusinov state [26–28] localized around a pointlike magnetic impurity [37]. The coherence peaks at $|E| = \bar{\Delta}$ can be found outside the magnetic segment $\rho > R_0$.

When the exchange potential increases to $V_0 = 2\bar{\Delta}$ in (e), the LDOS spectra show a complicated profile due to the spatial variation of the pair potential. The sharp subgap peak around $E = 0.7\bar{\Delta}$ exists for $0 < \rho < 1.8\xi_0$ and $\rho > 2.3\xi_0$. At the node of the pair potential $\rho = 2\xi_0$, the subgap peaks around $E = 0.7\bar{\Delta}$ are drastically suppressed and the LDOS shows almost flat spectra as it does in the normal state.

The same tendency can also be seen in the results for $V_0 = 3\bar{\Delta}$ in Fig. 2(f). The spectra of LDOS for $V_0 = 3\bar{\Delta}$ in (f) become more inhomogeneous and complicated than those in Figs. 2(d) and 2(e). At the outer node at $\rho = 2.2\xi_0$, the spectra are totally flat and LDOS does not have large peaks below the gap. At the inner node at $\rho = \xi_0$, however, the LDOS has a peak at zero energy. In Sec. IV, we will discuss the LDOS spectra being very sensitive to V_0 using the one-dimensional SF structure.

C. Pairing correlations

We display the pairing correlation functions in Figs. 2(g)–2(i) for $V_0 = \bar{\Delta}$, $2\bar{\Delta}$, and $3\bar{\Delta}$, respectively. The results are calculated for the lowest frequency $\omega_0 = \pi T$. The spin-singlet s-wave component for $V_0 = \bar{\Delta}$ is always larger than the other components and almost flat as shown in Figs. 2(g). Only this component has a finite amplitude far from the magnetic cluster. The two p-wave components show a broad peak at the boundary ($\rho = R_0$) as a result of the local inversion symmetry breaking. The odd-frequency triplet s-wave component has a relatively larger amplitude than the induced p-wave components around the center.

It is possible to derive the Eilenberger equation for corresponding four coherence functions: γ_0^{SW}, γ_0^{PW}, γ_3^{SW}, and γ_3^{PW}. The detailed results are displayed in the Appendix. The equation following the first row of Eq. (A5),

$$v_F k_x \frac{d}{dx}\gamma_0^{\text{SW}} + 2\omega_n\gamma_0^{\text{PW}} + 2V\gamma_3^{\text{PW}} = 0, \qquad (22)$$

indicates that the spatial variation of the pair potential (spin-singlet s-wave superconductor) generates two p-wave components γ_0^{PW} and γ_3^{PW}. In addition, the equation following the second row of Eq. (A5),

$$v_F k_x \frac{d}{dx}\gamma_0^{\text{PW}} + 2\omega_n\gamma_0^{\text{SW}} + 2V\gamma_3^{\text{SW}} = \Delta, \qquad (23)$$

explains the appearance of the spin-triplet s-wave component γ_3^{SW} even in a uniform pair potential. Here we summarize our knowledge of the relation between the frequency symmetry of Cooper pairs and their influence on the free energy and on the quasiparticle LDOS.

(I) Usual *even-frequency* pairs indicate the diamagnetic response to magnetic fields and favor the spatially uniform superconducting phase at the ground state. On the other hand, *odd-frequency* Cooper pairs are paramagnetic [60]. Therefore, odd-frequency pairs increase the free energy of the uniform ground state [61] and favor the spatial gradient of the superconducting phase [37].

(II) The LDOS has a gapped energy spectrum in the presence of even-frequency pairs, whereas it tends to have peaks below the gap in the presence of odd-frequency pairs [62,63].

These properties qualitatively explain the characteristic behavior in the free-energy density and those in the LDOS. The LDOS for $V_0 = \bar{\Delta}$ in Fig. 2(d) shows the gaplike energy spectra because even-frequency component f_0^{SW} is dominant everywhere. When the exchange potential increases to $V_0 = 2\bar{\Delta}$, a node appears in the pair potential. As a consequence, the spatial profile of the pairing correlations drastically changes as shown in Fig. 2(h). The two p-wave components have peaks inside the boundary because the pair potential and the exchange potential break the inversion symmetry locally. The amplitudes of the two p-wave components are larger than those in Fig. 2(g). The two spin-triplet components have large amplitudes around the node of the pair potential. The sign change of the pair potential is equivalent to the local π-phase shift in the pair potential. According to the property (I), odd-frequency spin-triplet s-wave components f_3^{SW} appear to decrease the free-energy density at the node of the pair potential. The triplet p-wave component f_3^{PW} is the most dominant at the node $\rho = 2\xi_0$. As a consequence, LDOS at the

node in Fig. 2(e) does not have large peaks below the gap. The two odd-frequency components are the source of the subgap peak at $E = 0.7\bar{\Delta}$ in Fig. 2(e) for $0 < \rho < 1.8\xi_0$. Outside the magnetic segment, f_0^{SW} is a source of the coherence peak at $E = \bar{\Delta}$ and f_0^{PW} assists the subgap peak at $E = 0.7\bar{\Delta}$. The two components f_0^{SW} and f_3^{PW} seem to affect the LDOS independently at $\rho > R_0$.

In a two-node state at $V_0 = 3\bar{\Delta}$, the pairing correlation functions oscillate beneath the magnetic cluster more rapidly as shown in Fig. 2(i). At the outer node $\rho = 2.2\xi_0$, the two spin-triplet components (f_3^{PW} and f_3^{SW}) have peaks. The spectra of LDOS show the flat structure because the amplitude of f_3^{PW} and that of f_3^{SW} are almost the same at the outer node. Around the inner node at $\rho = \xi_0$, the two odd-frequency pairing correlations have larger amplitudes than the two even-frequency pairing correlations. As a consequence, LDOS has a peak at zero energy for $0.7\xi_0 < \rho < 2.0\xi_0$. Therefore, the relative amplitudes among the four correlation functions govern the subgap spectra in the LDOS. When the odd-frequency (even-frequency) pairing correlations are dominant, the LDOS tends to have peak (gap) at $E < \bar{\Delta}$.

At the end of this subsection, we briefly summarize the two properties of the local FFLO states. First, zero-energy peaks appear at the edge of the ferromagnetic segment $\rho = R_0$ in Figs. 2(e) and 2(f). When V_0 is close to a transition point between the n-node and ($n \pm 1$)-node states, the LDOS tends to have a zero-energy peak at the boundary. However, this zero-energy peak is not universal and depends on the amplitude of the magnetization. We will further explore this issue in Sec. IV.

Secondly, Eq. (22) implies that the spatial variation of the singlet s-wave component (linked to the pair potential) generates two p-wave components. Simultaneously, we can state that the p-wave pairing correlations drive the spatial variation of the pair potential. Therefore, p-wave pairing correlations are indispensable to realizing the FFLO states. This insight is consistent with the fact that the FFLO states are fragile against impurity scatterings [64–66]. To our knowledge, a spin-singlet s-wave superconducting state is fragile when it contains odd-frequency pairing correlations in the clean limit [67,68].

D. Discontinuous transition

The spatial profiles of the pair potential with several radii of the magnetic cluster are shown in Fig. 3(a), where we choose $R_0/\xi_0 = 3, 5$, and 7 and $V_0 = 2\bar{\Delta}$. The results indicate that, if the radius of the magnetic cluster is large enough, the multinode states appear even with a weak exchange potential. In Figs. 3(b) and 3(c), we plot the pair potential at the center of the ferromagnetic segment $\Delta_c \equiv \Delta(\rho = 0)$ as a function of V_0 [69], where the radius varies from $R_0 = \xi_0$ to $6\xi_0$ by ξ_0 with the corresponding offset and the temperature is set to (b) $T/T_c = 0.2$ and (c) 0.1. The pair potential keeps the homogeneous profile (i.e., $\Delta_c \approx \bar{\Delta}$ without a node) until V_0 reaches a critical value, which we define V_1. At $V_0 = V_1$, Δ_c changes the sign abruptly, meaning that a node appears in the pair potential. Each time Δ_c changes the sign in Fig. 3, the number of nodes in the pair potential changes by one. The results show a relation $V_1 \approx \bar{\Delta}$ holds $R_0 > 2\xi_0$, which
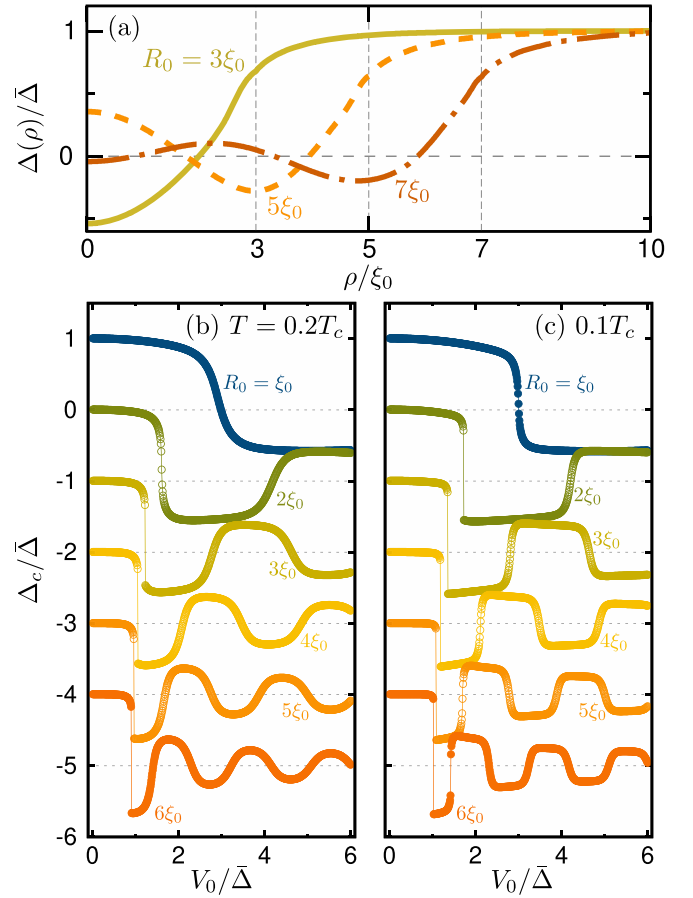

FIG. 3. (a) Cluster-size dependence of pair potentials at $V_0 = 2\bar{\Delta}$. (b),(c) Pair potential at the center of the magnetic cluster ($\rho = 0$) as a function of the exchange potential V_0. The radius of the cluster varies from $R = \xi_0$ to $6\xi_0$ by ξ_0. The results are plotted with the offset by $(R_0/\xi_0 - 1)\bar{\Delta}$. The horizontal broken lines indicate zeros. The temperature is set to (a),(b) $T = 0.2T_c$ and (c) $0.1T_c$.

limits the validity of the theoretical model for a topologically nontrivial superconducting nanowire [70,71].

We also find jumps in Δ_c at $V_0 = V_1$ show the hysteresis between the two processes in the numerical simulation: increasing and decreasing V_0. The results for $R_0 = 3\xi_0$ are displayed in Fig. 4, where we choose (a) $T = 0.2T_c$ and (b) $0.1T_c$. The hysteresis loop is more prominent at a lower temperature. We have confirmed that the hysteresis loop appears also between the one- and two-node states if the temperature is low enough.

Comparing Figs. 3(b) and 3(c), we see the discontinuous behavior is the more remarkable at the lower temperature. The first term of the Eilenberger equation (7) is $[\partial_x + (2\xi_T)^{-1}]\hat{\gamma}$ along the x coordinate, where we focus on the lowest Matsubara frequency and $\xi_T = \hbar v_F/2\pi T$ is the thermal coherence length in the clean limit. In this case, the length scale of the spatial variation of $\hat{\gamma}$ is approximately given by ξ_T. In other words, the spatial variation in the coherence functions are correlated within the range with $\pi \xi_T^2$. At $T = 0.1T_c$, the thermal coherence length becomes $\xi_T = 10\xi_0$, which covers the whole ferromagnetic segment. In this case, Δ prefers a homogeneous profile as much as possible until V_0 exceeds a critical value
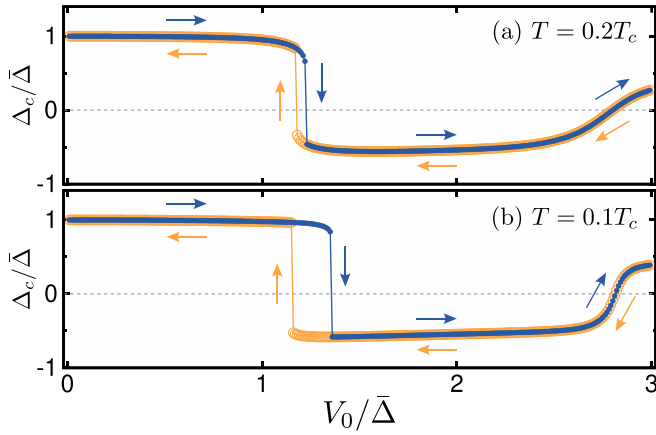
FIG. 4. Hysteresis loop of Δ_c. The degree of the hysteresis is more prominent for larger magnetic clusters and at lower temperatures. The arrows indicate how the exchange potential is changed in the numerical simulation. The radius of the island is set to $R_0 = 3\xi_0$.

because the influence of a node in the pair potential spreads over a wide region of approximately $\pi \xi_T^2$. Therefore, at low temperature, the jump in Δ_c is more abrupt. Figure 3 also indicates that the discontinuity between the zero-node and the one-node states is more remarkable for larger clusters. At present, however, we cannot think of reasons for this tendency.

In Fig. 5, we display the pairing correlation functions by changing the exchange potential gradually for $R_0 = 3\xi_0$. The spatial profile of the spin-singlet s-wave component in the n-node state is qualitatively different from those in $(n \pm 1)$-node states [Fig. 5(a)]. The spatial profiles of f appear to be insensitive to V_0 as long as the number of nodes in the pair potential remains the same value. As a result, the calculated results
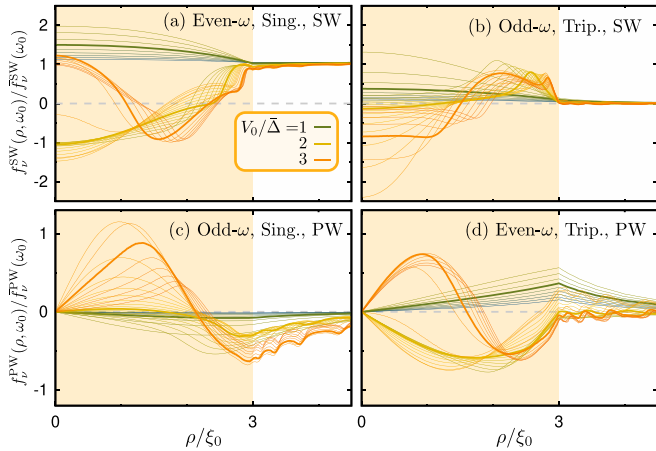

FIG. 5. Evolutions of pair amplitudes over magnetization. (a) Even-frequency spin-singlet s wave, (b) odd-frequency triplet s wave, (c) odd-frequency singlet p wave, and (d) even-frequency triplet p wave are shown. The spatial profile of the pair potential is qualitatively the same as those in (a), the principal component. The magnetization varies from $V_0/\bar{\Delta} = 0.5$ to 4.0 by 0.1. The radius of the island and the temperature are set to $R_0 = 3\xi_0$ and $T = 0.1T_c$. The even-frequency components (a),(d) exhibit discrete behavior, while the odd-frequency components (b),(c) vary gradually. The values of V_0 are given in the legend only for the thick lines.

for f_0^{SW} are bundled for each state. The same discontinuous behavior appears in the even-frequency spin-triplet p-wave component in Fig. 5(d). Such discontinuous behavior in the pairing correlation functions is responsible for the jump of the pair potential between the n-node state and $(n + 1)$-node state. The spatial profile of the two even-frequency pairing components is governed mainly by the number of nodes. The two odd-frequency components in Figs. 5(b) and 5(c), on the other hand, change gradually with increasing V_0. Consequently, odd-frequency pairs relax the effects of discontinuous change in the pair potential at the transition point. This might be a role of odd-frequency pairs in the FFLO states. The gradual change of the odd-frequency pairing correlations causes the gradual change of subgap spectra in the LDOS. We will discuss this issue in Sec. IV.

IV. ANALYSIS IN ONE-CHANNEL MODEL

The one-channel model is represented by putting $k_y = 0$ in all the equations in Sec. II and describes a one-dimensional superconducting structure including the exchange potential of $V(x) = V_0 \Theta(L_0 - |x|)$. Although the one-channel model is not realistic, the characteristic behaviors in the LDOS in the one-channel model are simpler than those in two dimensions.

The pair potential at the center of the system (i.e., $\Delta_c = \Delta|_{x=0}$) is shown in Fig. 6(a), where $L_0 = 3\xi_0$ and $T = 0.2T_c$. We focus on the several characteristic exchange potentials indicated by the arrows: $V_0/\bar{\Delta} = 0.8$ (zero node), 1.1 (just before the transition), 1.2 (just after the transition), 1.9 (one-node state), 2.9 (just after the second transition), and 3.8 (two-node state). The spatial profile of the pair potentials in Fig. 6(b) is qualitatively the same as those in the 2D case [see Figs. 2(a)–2(c)]. We have also confirmed that the transition between the one-node and two-node states becomes discontinuous at a low temperature (the results are not shown). The LDOS for the characteristic exchange potentials are shown in Figs. 6(c)–6(h). The LDOS indicate that the quasiparticle spectra are not simply determined by the number of nodes but depend sensitively on the exchange potential. In the zero-node state in Fig. 6(c), the LDOS at the interface ($x = 3\xi_0$) has peaks around $|E| = 0.6$ and that at the center of the magnetic segment has peaks around $|E| = 0.9$. Just below the transition point to the one-node state, the LDOS at the boundary ($x = 3\xi_0$) has a peak at zero energy as shown in Fig. 6(d). The zero-energy peak at the boundary can be seen also just above the transition point in Figs. 6(e) and 6(g). At $V_0/\bar{\Delta} = 1.9$, the one-node state is stable because the exchange potential is far from the two transition points at $V_0/\bar{\Delta} = 1.15$ and 2.85 [see Fig. 6(a)]. The corresponding LDOS [Fig. 6(f)] shows that the spectra are flat $N \approx N_0$ at the node of the pair potential and gapped at the boundary. The same behavior appears also for the stable two-node states at $V_0/\bar{\Delta} = 3.8$ [Fig. 6(h)]. Although the pair potentials for $V_0/\bar{\Delta} = 1.2$ and 1.9 have similar profiles, the subgap spectra [Figs. 6(e) and 6(f)] are qualitatively different. As already discussed in Fig. 5, the spatial profiles of the odd-frequency components for these states deviate from each other. As a result, the subgap spectra in Figs. 6(e) and 6(f) are totally different from each other according to property (II). The spatial profiles of the odd-frequency components are very sensitive to V_0 and those for these two states are qualitatively
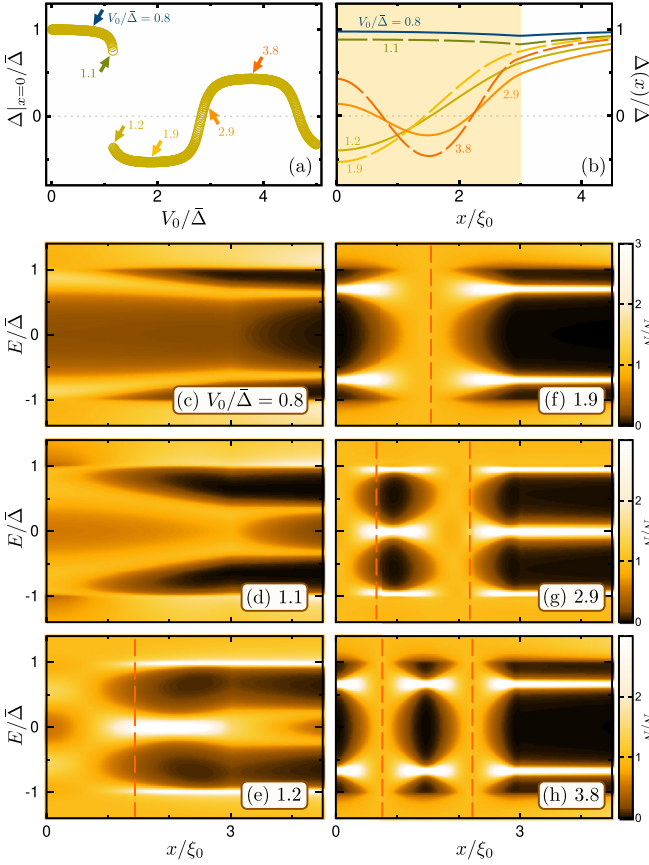
FIG. 6. Results for the one-channel model. The length of the ferromagnet and the temperature are set to $L_0 = 3\xi_0$ and $T = 0.2T_c$, respectively. (a) Pair potential at the center of the system. (b) Spatial profiles of the pair potential. (c)–(h) Local density of states. The magnetization is set to the characteristic values indicated by the arrows in (a): $V_0/\bar{\Delta} = 0.8$ (zero node), 1.1 (before the transition), 1.2 (after the transition), 1.9 (one-node state), 2.9 (after the second transition), and 3.8 (two-node state). The vertical broken lines in (c)–(h) indicate the position of the nodes.

different (the results are not shown but similar to those in Fig. 5). Therefore, the subgap spectra shown in Figs. 6(e) and 6(f) exhibit distinct differences, which can be attributed to property (II). This discussion can be applied also to the LDOS in the two two-node states shown in Figs. 6(g) and 6(h). Thus the gradual changes of the odd-frequency pairing correlations are responsible for the gradual changes in the LDOS.

V. CONCLUSION

We have theoretically studied the property of the Fulde-Ferrell-Larkin-Ovchinnikov (FFLO) state which appears in a superconducting thin film attached to a circular-shaped magnetic cluster. By solving the quasiclassical Eilenberger equation, we calculate the pair potential, free-energy density, the pairing correlation functions, and the local density of states. The FFLO states are locally realized beneath the ferromagnetic cluster as a stable solution of the self-consistent gap equation. The free-energy density shows that the local FFLO states are supported by the superconducting condensate surrounding the magnetic cluster. As the exchange potential

increases, the number of nodes in the pair potential increases one by one.

The spatial profiles of the even-frequency pairing correlations are not sensitive to the exchange potential and are determined mainly by the number of nodes in the pair potential. On the other hand, the odd-frequency pairing correlations show a gradual change with increasing the exchange potential. The local density of states is inhomogeneous in the local FFLO state. In addition, the subgap spectra depend sensitively on the exchange potential because the odd-frequency pairs coexist with subgap quasiparticles.

APPENDIX: ANALYSIS IN LINEARIZED EILENBERGER EQUATION

It is possible to derive the Eilenberger equation for the corresponding four coherence functions defined by

$$\gamma_0^{\mathrm{SW}} = \frac{1}{2}\{\gamma_0(\boldsymbol{k}) + \gamma_0(-\boldsymbol{k})\}, \tag{A1}$$

$$\gamma_0^{\mathrm{PW}} = \frac{1}{2}\{\gamma_0(\boldsymbol{k}) - \gamma_0(-\boldsymbol{k})\}, \tag{A2}$$

$$\gamma_3^{\mathrm{SW}} = \frac{1}{2i}\{\gamma_3(\boldsymbol{k}) + \gamma_3(-\boldsymbol{k})\}, \tag{A3}$$

$$\gamma_3^{\mathrm{PW}} = \frac{1}{2i}\{\gamma_3(\boldsymbol{k}) - \gamma_3(-\boldsymbol{k})\}. \tag{A4}$$

Here we assume that an s-wave (p-wave) component is the most dominant in an even-parity (odd-parity) coherence function. The Eilenberger equation for these components results in

$$
v_F \boldsymbol{k} \cdot \nabla
\begin{bmatrix}
\gamma_0^{\mathrm{SW}} \\
\gamma_0^{\mathrm{PW}} \\
\gamma_3^{\mathrm{SW}} \\
\gamma_3^{\mathrm{PW}}
\end{bmatrix}
+ 2
\begin{bmatrix}
0 & \omega & 0 & V \\
\omega & 0 & V & 0 \\
0 & -V & 0 & \omega \\
-V & 0 & \omega & 0
\end{bmatrix}
\begin{bmatrix}
\gamma_0^{\mathrm{SW}} \\
\gamma_0^{\mathrm{PW}} \\
\gamma_3^{\mathrm{SW}} \\
\gamma_3^{\mathrm{PW}}
\end{bmatrix}
$$

$$
+
\begin{bmatrix}
2(\gamma_0^{\mathrm{SW}}\gamma_0^{\mathrm{PW}} - \gamma_3^{\mathrm{SW}}\gamma_3^{\mathrm{PW}}) \\
(\gamma_0^{\mathrm{SW}})^2 + (\gamma_0^{\mathrm{PW}})^2 - (\gamma_3^{\mathrm{SW}})^2 - (\gamma_3^{\mathrm{PW}})^2 \\
2(\gamma_0^{\mathrm{SW}}\gamma_3^{\mathrm{PW}} + \gamma_0^{\mathrm{PW}}\gamma_3^{\mathrm{SW}}) \\
2(\gamma_0^{\mathrm{SW}}\gamma_3^{\mathrm{SW}} - \gamma_0^{\mathrm{PW}}\gamma_3^{\mathrm{PW}})
\end{bmatrix}
$$

$$
=
\begin{bmatrix}
0 \\
\Delta \\
0 \\
0
\end{bmatrix}. \tag{A5}
$$

The pair potential is calculated from the spin-singlet s-wave component γ_0^{SW}.

[1] P. Fulde and R. A. Ferrell, Phys. Rev. **135**, A550 (1964).

[2] A. I. Larkin and Y. N. Ovchinnikov, Zh. Eksp. Teor. Fiz. **47**, 1136 (1964) [Sov. Phys. JETP **20**, 762 (1965)].

[3] R. Lortz, Y. Wang, A. Demuer, P. H. M. Böttger, B. Bergk, G. Zwicknagl, Y. Nakazawa, and J. Wosnitza, Phys. Rev. Lett. **99**, 187002 (2007).

[4] S. Yonezawa, S. Kusaba, Y. Maeno, P. Auban-Senzier, C. Pasquier, K. Bechgaard, and D. Jérome, Phys. Rev. Lett. **100**, 117002 (2008).

[5] C. C. Agosta, J. Jin, W. A. Coniglio, B. E. Smith, K. Cho, I. Stroe, C. Martin, S. W. Tozer, T. P. Murphy, E. C. Palm, J. A. Schlueter, and M. Kurmoo, Phys. Rev. B **85**, 214514 (2012).

[6] M. D. Croitoru and A. I. Buzdin, Phys. Rev. B **86**, 064507 (2012).

[7] M. D. Croitoru and A. I. Buzdin, J. Phys.: Condens. Matter **25**, 125702 (2013).

[8] H. Mayaffre, S. Krämer, M. Horvatić, C. Berthier, K. Miyagawa, K. Kanoda, and V. Mitrović, Nat. Phys. **10**, 928 (2014).

[9] G. Koutroulakis, H. Kühne, J. A. Schlueter, J. Wosnitza, and S. E. Brown, Phys. Rev. Lett. **116**, 067003 (2016).

[10] S. Imajo, T. Kobayashi, A. Kawamoto, K. Kindo, and Y. Nakazawa, Phys. Rev. B **103**, L220501 (2021).

[11] S. Kasahara, Y. Sato, S. Licciardello, M. Čulo, S. Arsenijević, T. Ottenbros, T. Tominaga, J. Böker, I. Eremin, T. Shibauchi, J. Wosnitza, N. E. Hussey, and Y. Matsuda, Phys. Rev. Lett. **124**, 107001 (2020).

[12] S. Kasahara, H. Suzuki, T. Machida, Y. Sato, Y. Ukai, H. Murayama, S. Suetsugu, Y. Kasahara, T. Shibauchi, T. Hanaguri, and Y. Matsuda, Phys. Rev. Lett. **127**, 257001 (2021).

[13] K. Kinjo, M. Manago, S. Kitagawa, Z. Mao, S. Yonezawa, Y. Maeno, and K. Ishida, Science **376**, 397 (2022).

[14] S. Kitagawa, G. Nakamine, K. Ishida, H. S. Jeevan, C. Geibel, and F. Steglich, Phys. Rev. Lett. **121**, 157004 (2018).

[15] H. Burkhardt and D. Rainer, Ann. Phys. (Leipzig) **506**, 181 (1994).

[16] S. Matsuo, S. Higashitani, Y. Nagato, and K. Nagai, J. Phys. Soc. Jpn. **67**, 280 (1998).

[17] L. N. Bulaevskii, V. V. Kuzii, and A. A. Sobyanin, JETP Lett. **25**, 291 (1977).

[18] A. I. Buzdin, L. N. Bulaevskii, and S. V. Panyuko, Pis'ma Zh. Eksp. Teor. Fiz. **35**, 147 (1982) [JETP Lett. **35**, 179 (1982)].

[19] V. V. Ryazanov, V. A. Oboznov, A. Y. Rusanov, A. V. Veretennikov, A. A. Golubov, and J. Aarts, Phys. Rev. Lett. **86**, 2427 (2001).

[20] T. Kontos, M. Aprili, J. Lesueur, F. Genêt, B. Stephanidis, and R. Boursier, Phys. Rev. Lett. **89**, 137007 (2002).

[21] S. Mironov, A. Mel'nikov, and A. Buzdin, Phys. Rev. Lett. **109**, 237002 (2012).

[22] G. C. Ménard, S. Guissart, C. Brun, R. T. Leriche, M. Trif, F. Debontridder, D. Demaille, D. Roditchev, P. Simon, and T. Cren, Nat. Commun. **8**, 2040 (2017).

[23] G. C. Ménard, C. Brun, R. Leriche, M. Trif, F. Debontridder, D. Demaille, D. Roditchev, P. Simon, and T. Cren, Eur. Phys. J.: Spec. Top. **227**, 2303 (2019).

[24] G. C. Ménard, A. Mesaros, C. Brun, F. Debontridder, D. Roditchev, P. Simon, and T. Cren, Nat. Commun. **10**, 2587 (2019).

[25] A. A. Abrikosov and L. P. Gor'kov, Zh. Eksp. Teor. Fiz. **39**, 1781 (1960) [Sov. Phys. JETP **12**, 1243 (1961)].

[26] L. Yu, Acta Phys. Sin. **21**, 75 (1965).

[27] H. Shiba, Prog. Theor. Phys. **40**, 435 (1968).

[28] A. I. Rusinov, Zh. Eksp. Teor. Fiz. **56**, 2047 (1969) [JETP Lett. **9**, 85 (1969)].

[29] A. Yazdani, B. A. Jones, C. P. Lutz, M. F. Crommie, and D. M. Eigler, Science **275**, 1767 (1997).

[30] T.-P. Choy, J. M. Edge, A. R. Akhmerov, and C. W. J. Beenakker, Phys. Rev. B **84**, 195442 (2011).

[31] S. Nadj-Perge, I. K. Drozdov, J. Li, H. Chen, S. Jeon, J. Seo, A. H. MacDonald, B. A. Bernevig, and A. Yazdani, Science **346**, 602 (2014).

[32] A. I. Rusinov, Zh. Eksp. Teor. Fiz. **56**, 2047 (1969) [Sov. Phys. JETP **29**, 1101 (1969)].

[33] Y. V. Fominov and M. A. Skvortsov, Phys. Rev. B **93**, 144511 (2016).

[34] M. I. Salkola, A. V. Balatsky, and J. R. Schrieffer, Phys. Rev. B **55**, 12648 (1997).

[35] M. E. Flatté and J. M. Byers, Phys. Rev. Lett. **78**, 3761 (1997).

[36] A. V. Balatsky, I. Vekhter, and J.-X. Zhu, Rev. Mod. Phys. **78**, 373 (2006).

[37] S.-I. Suzuki, T. Sato, and Y. Asano, Phys. Rev. B **106**, 104518 (2022).

[38] D. Kuzmanovski, R. S. Souto, and A. V. Balatsky, Phys. Rev. B **101**, 094505 (2020).

[39] V. Perrin, F. L. N. Santos, G. C. Ménard, C. Brun, T. Cren, M. Civelli, and P. Simon, Phys. Rev. Lett. **125**, 117003 (2020).

[40] F. S. Bergeret, A. F. Volkov, and K. B. Efetov, Phys. Rev. Lett. **86**, 4096 (2001).

[41] R. S. Keizer, S. T. B. Goennenwein, T. M. Klapwijk, G. Miao, G. Xiao, and A. Gupta, Nature (London) **439**, 825 (2006).

[42] Y. Asano, Y. Tanaka, and A. A. Golubov, Phys. Rev. Lett. **98**, 107002 (2007).

[43] Y. Asano, Y. Sawa, Y. Tanaka, and A. A. Golubov, Phys. Rev. B **76**, 224525 (2007).

[44] V. Braude and Y. V. Nazarov, Phys. Rev. Lett. **98**, 077003 (2007).

[45] M. Eschrig and T. Löfwander, Nat. Phys. **4**, 138 (2008).

[46] J. W. A. Robinson, J. D. S. Witt, and M. G. Blamire, Science **329**, 59 (2010).

[47] T. S. Khaire, M. A. Khasawneh, W. P. Pratt, and N. O. Birge, Phys. Rev. Lett. **104**, 137002 (2010).

[48] M. S. Anwar, F. Czeschka, M. Hesselberth, M. Porcu, and J. Aarts, Phys. Rev. B **82**, 100501(R) (2010).

[49] G. Eilenberger, Z. Phys. A: Hadrons Nucl. **214**, 195 (1968).

[50] N. Schopohl, arXiv:cond-mat/9804064.

[51] N. Schopohl and K. Maki, Phys. Rev. B **52**, 490 (1995).

[52] M. Eschrig, Phys. Rev. B **61**, 9061 (2000).

[53] M. Eschrig, Phys. Rev. B **80**, 134511 (2009).

[54] In our configuration, a vortex state could be a possible solution of the Eilenberger equation. However, the vortex has typically a higher energy than the homogeneous state. Therefore, in this paper, we focus on the homogeneous superconductivity at $\rho \gg R_0$.

[55] Inversion symmetry is broken also by the spatially oscillating pair potential in the FFLO states. When the inversion symmetry is broken, parity is no longer a well-defined symmetry index. In other words, the parity mixing among even- and odd-parity pairing functions is allowed. Therefore, odd-parity pairs exist in the FFLO state of a spin-singlet even-parity superconductor.

[56] G. Eilenberger, Z. Phys. **190**, 142 (1966).

[57] S.-I. Suzuki and Y. Asano, Phys. Rev. B **91**, 214510 (2015).

[58] B. S. Chandrasekhar, Appl. Phys. Lett. **1**, 7 (1962).

[59] A. M. Clogston, Phys. Rev. Lett. **9**, 266 (1962).

[60] Y. Asano, A. A. Golubov, Y. V. Fominov, and Y. Tanaka, Phys. Rev. Lett. **107**, 087001 (2011).

[61] Y. Asano and A. Sasaki, Phys. Rev. B **92**, 224508 (2015).

[62] Y. Tanaka and A. A. Golubov, Phys. Rev. Lett. **98**, 037003 (2007).

[63] D. Kim, S. Kobayashi, and Y. Asano, J. Phys. Soc. Jpn. **90**, 104708 (2021).

[64] L. G. Aslamazov, Zh. Eksp. Teor. Fiz. **55**, 1477 (1968) [Sov. Phys. JETP **28**, 773 (1969)].

[65] S. Takada, Prog. Theor. Phys. **43**, 27 (1970).

[66] M. Houzet and V. P. Mineev, Phys. Rev. B **74**, 144522 (2006).

[67] Y. Asano and A. A. Golubov, Phys. Rev. B **97**, 214508 (2018).

[68] T. Sato and Y. Asano, Phys. Rev. B **102**, 024516 (2020).

[69] Changing V_0 in the horizontal axis is realized by applying an external Zeeman field in addition to the magnetic moment possessed in a ferromagnet.

[70] Y. Oreg, G. Refael, and F. von Oppen, Phys. Rev. Lett. **105**, 177002 (2010).

[71] R. M. Lutchyn, J. D. Sau, and S. Das Sarma, Phys. Rev. Lett. **105**, 077001 (2010).